

Analytical approximation of the two-dimensional percolation threshold for fields of overlapping ellipses

Y.-B. Yi and A. M. Sastry

Department of Mechanical Engineering, University of Michigan, Ann Arbor, Michigan 48109-2125

(Received 14 May 2002; published 20 December 2002)

Percolation of particle arrays is of high interest in microstructural design of materials. While there have been numerous contributions to theoretical modeling of percolation in particulate systems, no analytical approximation for the generalized problem of variable aspect-ratio ellipses has been reported. In the present work, we (1) derive, and verify through simulation, an analytical percolation approach capable of identifying the percolation point in two-phase materials containing generalized ellipses of uniform shape and size; and (2) explore the dependence of percolation on the particle aspect ratio. We validate our technique with simulations tracking both cluster sizes and percolation status, in networks of elliptical and circular particles. We also outline the steps needed to extend our approach to three-dimensional particles (ellipsoids). For biological materials, we ultimately aim to provide direct insight into the contribution of each single phase in multiphase tissues to mechanical or conductive properties. For engineered materials, we aim to provide insight into the minimum amount of a particular phase needed to strongly influence properties.

DOI: 10.1103/PhysRevE.66.066130

PACS number(s): 64.60.Ak

I. INTRODUCTION

The determination of minimum amounts of phases required for percolation is a key first step, for example, in designing materials for mechanical [1–3], filtration [4–6], and conductive [7–9] properties. Percolation concepts have also been used, at a systems level, to model disease transmission [10–13] and to design sensor arrays [14–16]. Mathematically, general percolation processes and phenomena have been studied since the early part of the last century via development of exact solutions for the percolation of particles in a finite or infinite field, and through Monte Carlo simulations of percolation of particles.

Two primary means of estimating percolation points have been used extensively. One general methodology involves the use of Monte Carlo simulations to assign particle placements in a given field, for a number of “realizations.” The resulting fraction of percolated cases is then used as the probability of percolation. The other general methodology involves performing a series expansion of an expression for mean cluster size or other statistical parameter in order to study the convergence properties of a series [17,18]. This “series expansion method” has been widely used as a powerful tool to study both lattice percolation and continuum percolation problems. It has been widely presumed, in fact, that such solutions to percolation problems are derivable only for a few special cases of ordered arrays of bonds and sites, or arrays of circular particles [19,20]. Percolation phenomena in other particle networks, e.g., arrays of fibers, have been investigated primarily using numerical models for specific cases (e.g., fiber aspect ratios, L/D).

Our present interests center on the design of heterogeneous materials containing various shapes of particles, including fibers, which we can view generally as high aspect-ratio elliptical or ellipsoidal particles. The fact that higher aspect ratio phases percolate at lower volume or area fractions than lower aspect ratio phases has been well docu-

mented. In early work, Kirkpatrick’s simulations [21] showed that the percolation threshold ρ_c , i.e., the density or volume fraction of the fiber phases at percolation onset, exhibited a power law dependence upon bond fraction ν , expressible as

$$\rho_c(\nu) \propto (\nu - \nu_c)^t. \quad (1)$$

This power law relation was also found to hold for conductivity in fiber arrays, near the percolation point. Pike and Seager [22] also examined conduction and percolation phenomena in stick networks (among others), using two-dimensional (2D) and three-dimensional (3D) Monte Carlo simulations; the effects of hard core interactions, probabilistic and deterministic bonding parameters, and various forms for the bonding function were specifically investigated.

Here we derive, and verify through simulation, an analytical percolation technique allowing the approximation of the percolation point in arrays of generalized ellipses, of uniform shape and size. For biological materials, we ultimately aim to provide direct insight into the contribution of each single phase in multiphase tissues to mechanical or conductive properties; this insight may ultimately be useful for validating selection hypotheses involving particular types or morphologies of tissue [23]. For engineered materials, we aim to provide insight into the minimum amount of a particular phase needed to strongly influence overall properties; this will probably be useful in the design of materials, e.g., the determination of the amount of additives needed for significant improvement of conductivity in composite media. We validate our solution using Monte Carlo simulations, and also using prior analytical techniques for circular particles (the simplest case in the present theoretical development).

II. BACKGROUND

A. Conduction, conductive additives, and percolation

The technological importance of design near the percolation point cannot be overstated; selection of minimum

amounts of additive phases reduces, cost, mass, and allows a greater choice of manufacturing approach. Sastry and co-workers [1,2,7,8, present work] have extensively investigated transport in stochastic fibrous networks through simulation and closed-form semiempirical approaches.

1. Aspect ratio, conduction, and percolation

A number of specific results were obtained for materials relevant to battery technologies, wherein fibers of aspect ratio of 50:1 and 100:1 were examined for their conductive properties [7]. For example, at lower volume fractions (2–10%) a significant advantage was found for use of high aspect-ratio fibers as conductive elements. For example, with no additional conductive mass, a fourfold increase in the aspect ratio (the ratio of fiber length L to diameter D) resulted in a 50-fold improvement in conductivity, at 5% volume fraction. Comparisons between two fiber types, having two different lengths relative to the simulation domain edge length L_u ($L/L_u=1, L/D=100$ and $L/L_u=1.5, L/D=100$), showed that the effective conductivity and variance in conductivity are both relatively insensitive to the alteration of staple length [7] in that regime of “window” sizes, or the relative length of the simulation domain edge to the particle size.

2. Property variance near the percolation point

As discussed, semiempirical models of percolation in complex particle arrays can be used to deterministically predict a single-valued conductivity at a given particle density, though the variance in conductivity of real or simulated arrays near the percolation point can be quite high [8]. The effect of the staple aspect ratio on variances in simulated effective conductivities was previously investigated using direct simulations of conduction in fiber arrays, with fibers of aspect ratio $L/D=10$ and 100 , respectively ($L/L_u=1.5$ in both cases) [8]. Variances were approximately 20 times greater in the former case, demonstrating that the variances were strongly influenced by fiber shape. Therefore, not only can significant improvements in conductivity be achieved with modest changes in fiber geometry, but variances can be much better controlled.

3. Comparison: Recent simulations with semiempirical approaches

Semiempirical approaches generally underestimate the conductivity of fiber arrays [21,24], as calculated from an exact resistor network approach. The percolation threshold for fibers of aspect ratios ~ 100 is around 4.2% [25,26] (and also confirmed by experimental observations, e.g., [27]). Percolation models are not valid below that point, though some low-density networks will percolate, with high variance in properties below the percolation point.

Clearly, simulations allow direct determination percolation properties of specific types of fiber arrays. Insight into the advantage of intermediate aspect ratio particles, for the full range between circles and high aspect ratio fibers, would be of high technological significance. Thus, we begin again with the problem of percolation in arrays of circles, and ex-

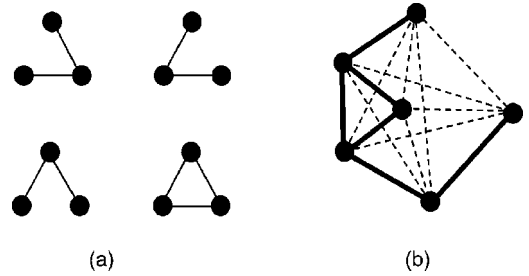


FIG. 1. Schematic of Penrose’s graph concept [33], showing (a) four possible *connected* graphs in a three-site problem, and (b) a *connected* graph A (formed by solid lines) and a *disconnected* graph B (formed by dashed lines) in a random graph G consisting of six sites, $G=A+B$.

tend the analytical result to ellipses; the aim is to span the understandings gained from analytical approaches in circular arrays, and direct simulation in fiber arrays, so that variance in percolation, and dependence upon aspect ratio, can be better explored analytically.

B. Estimation of the percolation point: Circular particles

The earliest investigation of this problem is attributable to Hann and Zwanzig [28], who used a power series in number density to systematically study the distribution of cluster size for overlapping circles and squares in two dimensions, as well as spheres and cubes in three dimensions. Coniglio *et al.* [17,18] developed a general formalism to obtain a closed form series expansion of the average number of clusters of particles. That work followed Hill’s initial efforts [29] studying physical clusters with a diagrammatic expansion, to determine correlation functions. Similar expressions have also been reported using graph theory [28] and the continuum Potts model (CPM) [30]. In this section we briefly reiterate the approach of the earlier workers [31–33] for determination of the percolation threshold for arrays of spatially uncorrelated, 2D circles.

Assuming circles are positioned at $\{r_1, r_2, \dots, r_k\}$ respectively, we define the function $g(r_i, r_j)$ as the probability that two circles positioned at r_i, r_j are connected, by closing the edge $\{r_i, r_j\}$. We define graph G as a cluster formed by connecting each points (r_i, r_j) in $\{r_1, r_2, \dots, r_k\}$ to the group; an illustration of the connected graph concept is given as Fig. 1. We find by the arrival method [31,43] that the number of possible ways to connect k particles is

$$\sum_{1=k_0 < k_1 < \dots < k_i = k} \{C_{k_i - k_0}^{k_1 - k_0} \dots C_{k_i - k_{i-1}}^{k_{i-1} - k_{i-2}}\} 2^{[C_{k_1 - k_0}^2 + \dots + C_{k_i - k_{i-1}}^2]} \times \{(2^{k_1 - k_0} - 1)^{k_2 - k_1} \dots (2^{k_{i-1} - k_{i-2}} - 1)^{k_i - k_{i-1}}\}, \quad (2)$$

with

$$C_i^j = \frac{i(i-1) \dots (i-j+1)}{j!}, \quad (3)$$

or equivalently,

$$\sum_{1=k_0 < k_1 < \dots < k_i = k} \frac{(k-1)!}{(k_1-k_0)! \dots (k_i-k_{i-1})!} \times 2^{[k_0-k_i+(k_1-k_0)^2+\dots+(k_i-k_{i-1})^2]/2} \times (2^{k_1-k_0}-1)^{k_2-k_1} \dots (2^{k_{i-1}-k_{i-2}}-1)^{k_i-k_{i-1}}. \quad (4)$$

There are four possible ways to connect three particles, and 38 ways to connect four particles (Hill [29]). This result can be used to verify Eq. (4).

We define function g_1 as the probability that a circle centered at r is connected to the graph G , which is formed by closing edges (r_i, r_j) in $\{r_1, r_2, \dots, r_k\}$. That is,

$$g_1(r; r^{(k)}) = g_1(r; r_1, r_2, \dots, r_k) = 1 - \prod_{j=1}^k [1 - g(r, r_j)]. \quad (5)$$

We define g_2 as the probability that the graph G is connected, per

$$g_2(r^{(k)}) = g_2(\{r_1, r_2, \dots, r_k\}) = \sum \left(\prod_A g(r_i, r_j) \prod_B [1 - g(r_i, r_j)] \right), \quad (6)$$

where the summation is taken over all *connected* graphs A on $\{r_1, r_2, \dots, r_k\}$. The first product is over all edges in A ; the second product is over all edges located in $B = G - A$.

We use the customary definition of a cluster, i.e., a cluster is an isolated group of particles in which there exists at least one unblocked path between any two member particles. Using this definition, and the definitions of functions g_1 and g_2 , Penrose [33] independently derived an integral expression for the probability that an arbitrary Poisson particle lies in a cluster consisting of k particles (or equivalently, a formula for the density of such clusters), using the conventional theory of statistics.

A brief description of Penrose's technique follows. Assuming that the first particle r_1 is fixed at the origin of the coordinate system, the probability that k particles are found in small regions around points $\{r_2, \dots, r_k\}$ is given by

$$\rho ds_2 \rho ds_3 \dots \rho ds_k = \rho^{k-1} ds_2 ds_3 \dots ds_k, \quad (7)$$

where ρ is particle density and s is area. The probability that these k particles form a cluster is

$$g_2(r^{(k)}). \quad (8)$$

From the theory of statistics, the probability that no Poisson point is bonded to any of $\{r_1, r_2, \dots, r_k\}$ (i.e., the probability that the cluster is isolated) can be expressed as

$$e^{-\rho \int g_1(r; r^{(k)}) ds}. \quad (9)$$

A combination of these expressions yields the probability that an arbitrary Poisson particle lies in a cluster consisting of k particles as

$$P_k = \frac{\rho^{k-1}}{(k-1)!} \int ds_2 \int ds_3 \dots \int ds_k e^{-\rho \int g_1(r; r^{(k)}) ds} g_2(r^{(k)}), \quad (10)$$

where the factorial term reflects the interchangeability of the particle positions within the cluster. The above equation is equivalent to the expression proposed by Penrose [33].

The percolation threshold can be evaluated after expanding the expression for mean cluster size, in a series. The convergence properties of the series can then be determined as functions of bonding criteria. Quintanilla and Torquato [31,32] used Penrose's integral expression [33] to evaluate cluster properties for arrays of circles, and obtained power series expansions for cluster properties to estimate percolation threshold. We define "mean cluster density" n_k as the particle-averaged number of clusters containing k particles, and n_k can be written

$$n_k = P_k / k = 1/k \left\{ \frac{\rho^{k-1}}{(k-1)!} \int ds_2 \int ds_3 \dots \int ds_k \times e^{-\rho \int g_1(r; r^{(k)}) ds} g_2(r^{(k)}) \right\}, \quad (11)$$

or alternatively expressed in Taylor series expansion following the approach of Quintanilla and Torquato [31,32] as

$$n_k = P_k / k = \sum_{i=0}^{\infty} (-1)^i \frac{\rho^{k-1+i}}{k^2 (k-1)! i!} \int ds_2 \int ds_3 \dots \int ds_k \times \left[\int g_1(r; r^{(k)}) ds \right]^i g_2(r^{(k)}). \quad (12)$$

The evaluation of each coefficient in the series in Eq. (12) requires the same amount of computational effort as the direct computation of n_k via Eq. (11). The coefficients can be used to obtain the low density expansions of the cluster statistics, including mean cluster size S and average cluster number Q , via

$$S = \sum_{k=1}^{\infty} k P_k = \sum_{k=1}^{\infty} k^2 n_k = \sum_{i=0}^{\infty} c_i \rho^i \quad (13)$$

and

$$Q = 1 / \sum_{k=1}^{\infty} n_k = 1 / \sum_{i=0}^{\infty} a_i \rho^i = \sum_{i=0}^{\infty} b_i \rho^i, \quad (14)$$

where coefficients b_i and a_i are related as

$$\begin{aligned}
 b_0 &= \frac{1}{a_0}, \\
 b_1 &= -\frac{a_1}{a_0^2}, \\
 b_2 &= -\frac{a_2}{a_0^2} + \frac{a_1^2}{a_0^3}, \\
 b_3 &= -\frac{a_3}{a_0^2} + \frac{2a_1a_2}{a_0^3} - \frac{a_1^3}{a_0^4}, \\
 &\dots
 \end{aligned} \tag{15}$$

The percolation thresholds can be estimated by checking the convergence criteria of the power series of the above cluster statistics. This can be done efficiently using the Pad approximants [34], in which the power series is approximated as a ratio of two series, with the denominator being a series of order one. For example, we can obtain

$$S = \sum_{i=0}^{\infty} c_i \rho^i = \frac{\sum_{i=0}^m A_i \rho^i}{B_0 + B_1 \rho} + O(\rho^{m+2}). \tag{16}$$

The percolation threshold is reached when the series S diverges. Therefore,

$$\rho_c \approx -\frac{B_0}{B_1}. \tag{17}$$

III. METHODS

A. Approximation of the analytical solution

1. Integral expression for the problem of oriented particles

Penrose's formula for the density of clusters was derived in the context of Poisson points. In fact, the formula can be extended to the more general problem in which particles with a fixed shape are oriented at random angles. To do so, we introduce an additional degree of freedom θ to the expression for cluster density. For the ellipse problem, in particular, θ can be defined as the inclination angle of the major axis with respect to the horizon, as shown in Fig. 2. The integration is thus performed over $r(x, y, \theta)$ instead of $r(x, y)$.

The previous integral equations assumed that particles were identical. However, we can also introduce probability distribution functions for any geometric parameter describing the particles (e.g., radii), in the integrand, as

$$\begin{aligned}
 n_k &= \frac{\rho^{*k-1}}{k!} \int \dots \int f(l_1^{(1)}, l_2^{(1)}, \dots) \\
 &\times f(l_1^{(2)}, \dots) \dots e^{-\rho^* f \dots f(l_1^{(r)}, l_2^{(r)} \dots) g_1(r; r^{(k)}) dl_1 dl_2 \dots ds} \\
 &\times g_2(r^k) dl_1^{(1)} dl_2^{(1)} \dots dl_1^{(2)} dl_2^{(2)} \dots ds_2 ds_3 \dots ds_k,
 \end{aligned} \tag{18}$$

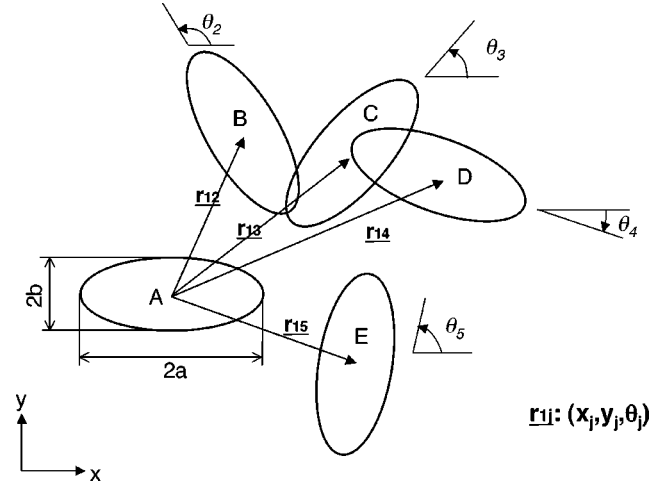


FIG. 2. Schematic of the geometric information required for the equisized ellipse problem. The orientation angle θ is zero for ellipse A, and $-\pi \leq \theta \leq \pi$ for other ellipses.

where l_n is a probability distribution function. Note in this formula that ρ is replaced by $\rho^* = \rho/\pi$, when the integration domain is $\theta \in (0, \pi)$. For the problem of identical ellipses whose geometric centers are positioned according to Poisson process, we have explicitly

$$\begin{aligned}
 n_k &= \frac{\rho^{*k-1}}{k!} \int dx_2 \int dy_2 \int d\theta_2 \dots \int dx_k \int dy_k \\
 &\times \int d\theta_k e^{-\rho^* \int g_1(r; r^{(k)}) dx dy d\theta} g_2(r^{(k)}),
 \end{aligned} \tag{19}$$

where x_i , y_i , θ_i are the x position, y position, and orientation angle, respectively, for the i th ellipse, $i=2, \dots, k$.

2. Bonding criterion for ellipses

For two circles, the bonding, or overlap, criterion may be written as simply $d \leq R_1 + R_2$, where R_1 and R_2 are the radii of the two particles, and d is the distance between their centers. For ellipses, the connection status can be analogously determined by the numerical solution of their combined equations, as

$$\begin{aligned}
 &\frac{[(x-x_i)\cos\theta_i + (y-y_i)\sin\theta_i]^2}{a^2} \\
 &+ \frac{[(x-x_i)\sin\theta_i - (y-y_i)\cos\theta_i]^2}{b^2} - 1 = 0
 \end{aligned} \tag{20}$$

on a particle-by-particle basis. The existence of real solutions implies that the two particles are connected. This method is tractable only for relatively small-scale problems; for practical materials systems, the approach is extremely computationally intensive. In view of this, an alternative method was developed. We assign one of the particles a zero orientation angle, then eliminate one of the unknowns in the governing equations of two ellipses, leading to an equation with a single unknown. The sign of the corresponding function value is then checked within the domain. The two particles

are connected if the sign changes at least once throughout the domain or the function has a zero value somewhere. In the case of identical ellipses, an even more efficient algorithm involving a contact function [35,36] can be introduced to determine whether the ellipses overlap or not: assuming one ellipse is centered at the origin and one is centered at (x_0, y_0) with relative orientation θ , the contact function is defined as

$$\Psi = 4(H_1^2 - 3H_2)(H_2^2 - 3H_1) - (9 - H_1H_2)^2, \quad (21)$$

where

$$H_1 = 3 + (\gamma - 1/\gamma)^2 \sin^2 \theta - (x_0/a)^2 - (y_0/b)^2 \quad (22)$$

and

$$H_2 = 3 + (\gamma - 1/\gamma)^2 \sin^2 \theta - (x_0 \cos \theta + y_0 \sin \theta)^2/a^2 - (y_0 \cos \theta - x_0 \sin \theta)^2/b^2. \quad (23)$$

If Ψ is negative, the two ellipses overlap. The two ellipses overlap if and only if Ψ , H_1 and H_2 are all positive. If $\Psi = 0$, the two ellipses are tangent. A contact function for differently sized ellipses can also be derived, and will be presented as part of future work. In computer realization, inputs include lengths of the major and minor axes, and orientation angles of each ellipse pair; Eqs. (21) through (23) are used to determine if the pair overlap.

3. The integration method

For the circle problem, evaluation of the integrals requires knowledge of the union area of k circles. Kratky [37] showed that the area of intersection of four or more circles can be determined via linear combination of the areas of intersection of two or three circles. Using this result, the union volume can also be determined exactly, and n_k can be obtained with an excellent accuracy. In the ellipse problem, however, there is no such equivalent and an integrand expression is not available explicitly; the integrals must be evaluated by definition. But we note that the integration domain can be greatly reduced by restricting calculations to the relatively small portion of the space in which particles are connected.

B. Simulation algorithm

In our simulations i identical elliptical particles were placed in a unit cell via random generations of centerpoints (x_i, y_i) and major axis orientations (q_i) , restricting centerpoints to those lying in the simulation window. We verified that the extraneous particle ends lying outside the simulation window introduced negligible error in calculated volume fractions.

1. Determination of cluster properties

The computational algorithm for determining n_k follows from the definition of a cluster. For each case, the total number of clusters of size k ($k=1,2,\dots$) is counted, and n_k is then simply the total cluster numbers of size k divided by the total number of particles in the system.

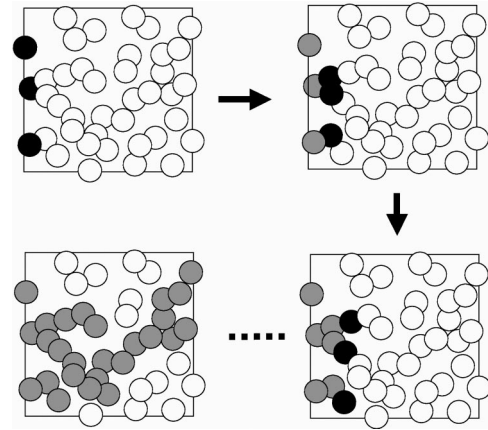


FIG. 3. Schematic depiction of the simulation algorithm for identifying percolation in a stochastic network system.

2. Detection of percolation

A variety of techniques, including the so-called “burning algorithm,” or “forest-fire model,” for lattice percolations [38–40] have been developed to determine percolation status of a network. Here, we introduce an analogous algorithm, shown schematically in Fig. 3. The particles in contact with an arbitrary side of the window are first identified. These particles (black circles) are assigned to class A. The remainder of the particles in the network (white circles) are assigned to class B. Connections between classes A and B are then examined. Members of B intersecting members of A are reassigned to class A; the original members of A (gray circles) are reassigned to class C. The process is repeated until no additional connections are found among members of A and B. A system is percolated if and only if particle class C spans opposite sides of a simulation window. The percolation probability for the network, p , is then simply m/n , where n is the total number of simulations, and m is the number of simulations in which percolation occurred.

C. Validation of analytical approach

Analytical approximations of cluster densities were compared to those obtained by simulations. A standard unit simulation window containing circles of diameter 0.04 were used in the simulations. Good agreements were obtained, with a maximum difference of less than 6% for cluster densities n_1 , n_2 , and n_3 . These results were also compared to those obtained by other researchers, including Quintanilla [31,32] and Hann [28]; good agreement was observed in both cases as well. Comparisons of percolation thresholds obtained analytically and numerically are presented in Fig. 4. The agreement is also acceptable, with an error less than 10% of the threshold value.

The error arises from several sources. First, the analytical approach assumes an infinite window size. Second, the simulation results were obtained using a finite number of computer simulations, and thus are themselves statistical quantities. Third, percolation thresholds were analytically estimated by truncating the power series expression, taking the first few terms as an approximation; thus, the numerical

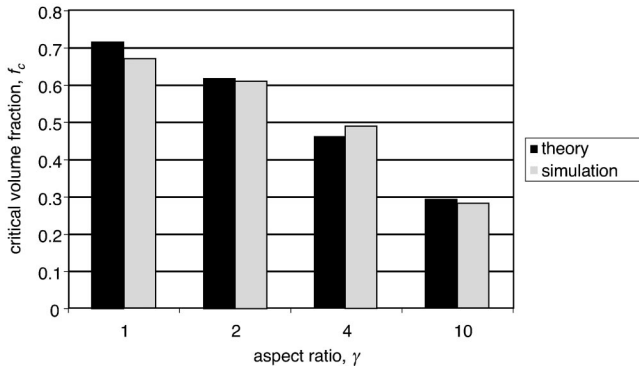


FIG. 4. Validation of the analytical solution with simulations for percolation thresholds arising in circular and elliptical arrays (various aspect ratios).

integration required in the analytical approach lead to an unavoidable inaccuracy. Reduction of this error can be obtained by using smaller integration intervals, which, naturally, reduces computational efficiency.

IV. DISCUSSION

Development of improved techniques for the prediction of percolative properties of multiphase materials is critical. Multiphase materials not only are utilized widely in exploiting multiple functionalities in engineered materials, but are also abundant in most functional biomaterials. In biomaterials, multiple phases are physiologically necessary, for example, to simultaneously maintain metabolic function, withstand mechanical loads, and accomplish self-repair. In both natural and engineered materials, the first important task in the analysis of mechanics or transport properties is to determine which phases are “percolated,” i.e., form continuous, domain-spanning paths from one boundary of interest to another. In biomaterials, this analysis can help determine which phases may be selected, in an evolutionary context, for their contribution to mechanical properties of a heterogeneous medium [41,42].

A. Effect of particle aspect ratio

It is well known that particle shape strongly affects cluster statistics and percolation probability in network systems. Figure 5 shows typical simulation results for cluster density in the overlapping circle problem. The error bars are standard deviations for simulations performed at a given volume fraction. At low density, most particles are isolated, and therefore smaller clusters dominate; at high density, however, particles are likely to be interconnected and thus larger clusters dominate. There exists a certain volume fraction f_k at which the cluster density is maximized; this volume fraction varies for clusters with different size, for instance, $f_1=0$ and $f_2=0.18$. Figure 6 shows how the aspect ratio affects the cluster density. As the particle aspect ratio increases, there are more possible ways for particles to connect, thus the number of clusters of size k ($k > 1$) increases at low volume fraction,

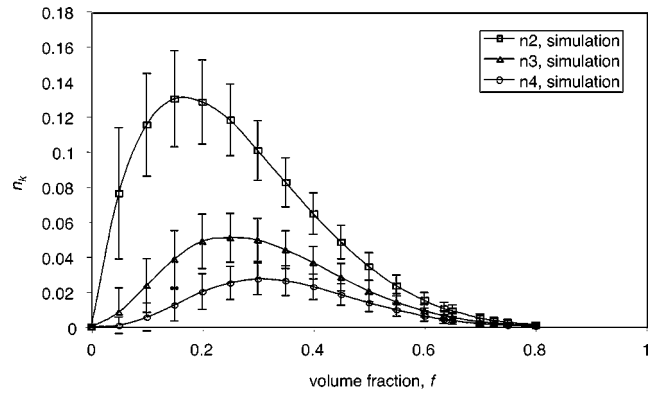


FIG. 5. Simulation results for cluster density for arrays of circles. The simulation window is a unit square; circular particles are of radius 0.05. Averaged results for 2000 simulations are shown at each point, with error bars for $\pm 1\sigma$ (standard deviation). n_k is the number of clusters of size k divided by the total number of circles.

and smaller clusters disappear at high volume fractions. Thus, the curves are shifted to smaller volume fractions with increasing aspect ratio.

In one of our parametric studies of percolation probability, the particle shape was altered such that the area of the particle was held constant for various aspect ratio particles. This study is relevant for applications in which, for example, the conductive mass is limited, but high conductivity is desired, and so acceptable particle shapes must be selected. Our results show that p increases monotonically with volume fraction f , and that the p - f curve appears to shift horizontally with an unchanged slope, as shown in Fig. 7. This implies that the slope is a function of particle area only, while the position of the p - f curve is related to γ . That is, we postulate

$$p = \Phi(f + \Gamma(\gamma), \lambda), \tag{24}$$

where we define the ratio of the major and minor ellipse axes (i.e., the aspect ratio) as $\gamma = a/b$ and $\lambda = 1/R$; R is the equivalent particle radius, or $R = \sqrt{ab}$.

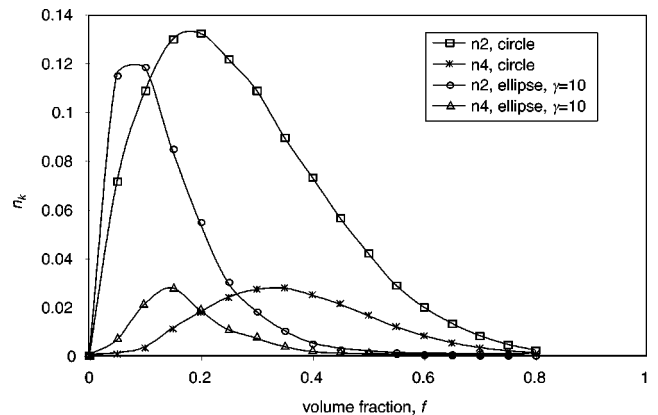


FIG. 6. Comparison of simulation results for circular and elliptical arrays, wherein both ellipses and circles are of area 0.0025. Circle radii are 0.05; ellipses have minor axes $a=0.158$ and major axes $b=0.0158$.

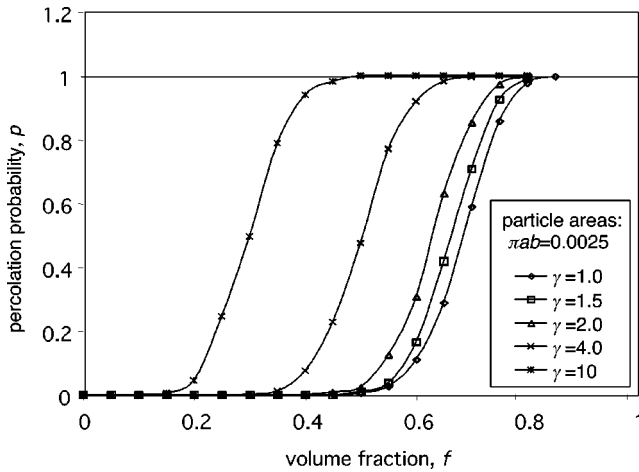


FIG. 7. Effect of the particle aspect ratio on percolation probability for elliptical arrays. Equivalent particle radius $R = \sqrt{ab} = 0.05$. Averaged results for 1000 simulations are shown at each point.

In another parametric study, we studied the effect of particle shape on percolation probability by changing the length of the major axis while the minor axis was held constant; thus, the particle area changed for different aspect ratios. We found that the slope of the p - f curve changed as the aspect ratio changed, as shown in Fig. 8, consistent with our previous finding that the slope of the p - f curve was a function of the particle area alone.

We must point out that the expressions of function Φ and Γ require knowledge about the two-point connectedness function [43–45]. In fact,

$$p = \int \int C(x_1, x_2) dx_1 dx_2 \quad (25)$$

where x_1 and x_2 denote the two boundaries at the direction of percolation. Once the two-point connectedness function $C(x_1, x_2)$ is known, it is fairly simple to evaluate p . However, the derivation of C is beyond the scope of this research and will be likely discussed in a future paper.

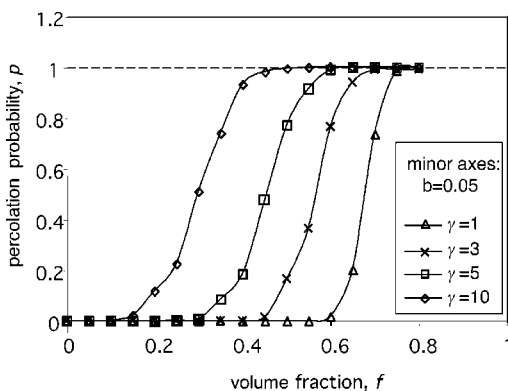


FIG. 8. Effect of the particle aspect ratio on percolation probability for elliptical arrays. The minor axis b is 0.05 for all cases. Averaged results for 1000 simulations are shown at each point.

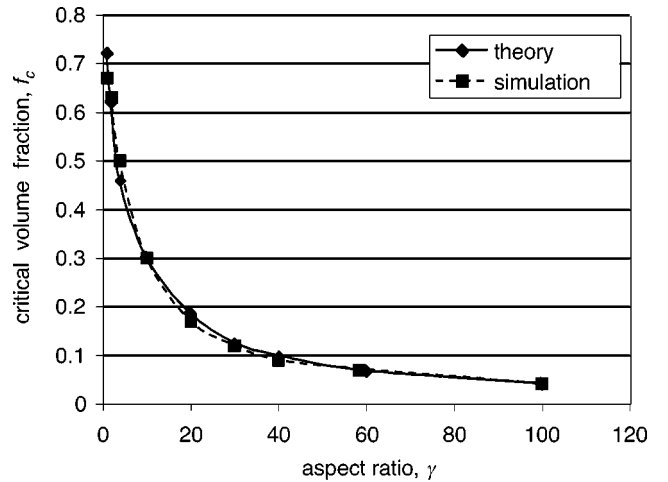


FIG. 9. Comparison of percolation thresholds determined via an analytical solution and simulation for the elliptical arrays. Analytical solutions were obtained using the series expansion method. Simulation results are from Xia [37].

In the case of an infinite domain, the percolation threshold, in terms of volume fraction, is irrelevant to the particle size, and can be expressed as a function of the aspect ratio from the analytical solution. Figure 9 shows how the percolation threshold changes with the aspect ratio, using the series expansion technique. Also shown in Fig. 9 are the simulation results obtained by Xia [36] for comparison. The two curves show good agreement. “Mild” ellipses, with the aspect ratio $1 < \gamma < 1.4$, exhibit percolation thresholds almost exactly those of circles, although the analytical approach suggests that there is some change in the percolation threshold due to γ even in these cases.

B. Effect of window size

For an infinite domain, percolation status is binary and deterministic: the network has only one status—percolated or not percolated. For percolated cases, a cluster of infinite size

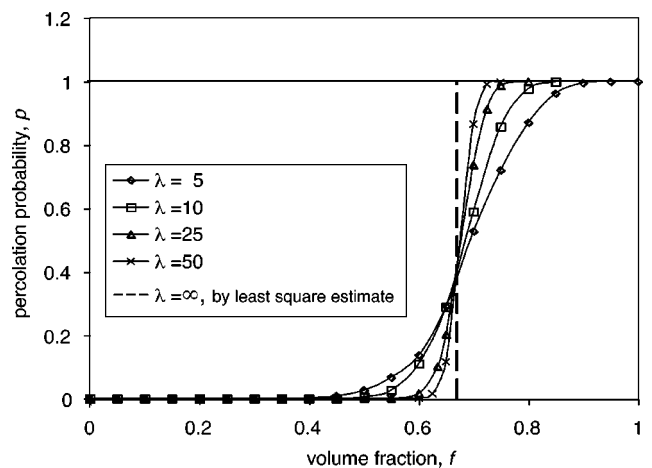


FIG. 10. Effect of particle size on percolation probability in elliptical arrays. $\lambda = 1/R$, and R represents equivalent particle radius $R = \sqrt{ab}$.

exists somewhere in the network, and the probability of percolation is one. For unpercolated cases, only finite clusters arise, and the probability of percolation is zero.

For a finite domain, however, the percolation status is probabilistic. Figure 10 shows the dependence of the percolation probability on the window size for the uniform circle problem. We studied this problem by varying the circle diameter while maintaining constant window size. The percolation probability P is a function of both λ and γ . We find that the slope of the probability curve becomes vertical as the window size increases. When the window size becomes infinitely large, the curve has a sudden jump at $f_c=0.67$ and the percolation probability curve is reduced to a step function at the percolation threshold f_c , indicating the system is unconditionally percolated when $f \geq f_c$ and not percolated

when $f \leq f_c$. The effect of particle size (or equivalently, the relative window size) on mean cluster density was also examined here, with only a slight effect observed. Thus, we conclude that the boundary conditions generally do not have significant effects on statistical cluster properties in terms of mean values, but do alter standard deviations.

ACKNOWLEDGMENTS

Support for this work, provided by DARPA and ONR through the Synthetic Multifunctional Materials (SMFM) Program (Dr. Leo Christodoulou and Dr. Steve Fishman) is gratefully acknowledged. Support from an NSF PECASE (A.M.S.) is also gratefully acknowledged.

-
- [1] A. M. Sastry, X. Cheng, and C. W. Wang, *J. Thermoplastic Composite Mater.* **11**, 288 (1998).
- [2] X. Cheng, C. W. Wang, A. M. Sastry, and S. B. Choi, *ASME J. Eng. Mater. Technol.* **121**, 514 (1999).
- [3] C. W. Wang, X. Cheng, A. M. Sastry, and S. B. Choi, *ASME J. Eng. Mater. Technol.* **121**, 503 (1999).
- [4] N. P. Niel and V. Privman, *Phys. Rev. A* **45**, 6099 (1992).
- [5] P. Deckmyn, G. Davies, and D. Bell, *Appl. Math. Model.* **19**, 258 (1995).
- [6] S. Datta and S. Redner, *Int. J. Mod. Phys. C* **9**, 1535 (1998).
- [7] X. Cheng and A. M. Sastry, *Mech. Mater.* **31**, 765 (1999).
- [8] X. Cheng, A. M. Sastry, and B. E. Layton, *ASME J. Eng. Mater. Technol.* **123**, 12 (2001).
- [9] S. Mohanty and M. Sharma, *Phys. Lett. A* **154**, 475 (1991).
- [10] H. K. Janssen, K. Oerding, F. van Wijland, and H. J. Hilhorst, *Eur. Phys. J. B* **7**, 137 (1999).
- [11] N. Zekri and J. P. Clerc, *Phys. Rev. E* **64**, 056115 (2001).
- [12] M. A. Fuentes and M. N. Kuperman, *Physica A* **267**, 471 (1999).
- [13] G. J. Gibson, *Appl. Stat.* **46**, 215 (1997).
- [14] L. A. L. de Almeida, G. S. Deep, A. M. N. Lima, and H. Neff, *Appl. Phys. Lett.* **77**, 4365 (2000).
- [15] D. E. Williams and K. F. E. Pratt, *Sens. Actuators B* **70**, 214 (2000).
- [16] G. Blaser, T. Ruhl, C. Diehl, M. Ulrich, and D. Kohl, *Physica A* **266**, 218 (1999).
- [17] A. Coniglio, U. Deangelis, A. Forlani, and G. Lauro, *J. Phys. A* **10**, 219 (1977).
- [18] A. Coniglio, U. Deangelis, and A. Forlani, *J. Phys. A* **10**, 1123 (1977).
- [19] M. F. Sykes and J. W. Essam, *Phys. Rev. Lett.* **10**, 3 (1963).
- [20] A. Drory, *Phys. Rev. E* **55**, 3878 (1997).
- [21] S. Kirkpatrick, *Rev. Mod. Phys.* **45**, 574 (1973).
- [22] G. E. Pike and C. H. Seager, *Phys. Rev. B* **10**, 1421 (1974).
- [23] Y. Yi, H. Wang, A. M. Sastry, and L. Lamberson, in *Smart Structures and Materials 2002: Industrial and Commercial Application of Smart Structures Technologies*, edited by A.-M. R. McGowan, Proc. of SPIE Vol. 4698 (SPIE, Bellingham, WA, in press), p. 212.
- [24] D. Stauffer, *Phys. Rep.* **54**, 1 (1979).
- [25] I. Balberg and N. Binenbaum, *Phys. Rev. B* **28**, 3799 (1983).
- [26] I. Balberg and N. Binenbaum, *Phys. Rev. Lett.* **52**, 1465 (1984).
- [27] A. M. Sastry, Sandia Report SAND94-2884 (1994).
- [28] S. W. Haan and R. Zwanzig, *J. Phys. A* **10**, 1547 (1977).
- [29] T. L. Hill, *J. Chem. Phys.* **23**, 617 (1955).
- [30] A. Drory, *Phys. Rev. E* **54**, 5992 (1996).
- [31] J. Quintanilla and S. Torquato, *Phys. Rev. E* **54**, 5331 (1996).
- [32] J. Quintanilla and S. Torquato, *Adv. Appl. Probab.* **29**, 327 (1997).
- [33] M. D. Penrose, *Adv. Appl. Probab.* **23**, 536 (1991).
- [34] G. A. Baker and P. Graves-Morris, *Padé Approximants*, 2nd ed. (Cambridge University Press, New York, 1995).
- [35] J. V. Baron, *J. Chem. Phys.* **56**, 4730 (1972).
- [36] W. Xia and M. F. Thorpe, *Phys. Rev. A* **38**, 2650 (1988).
- [37] K. W. Kratky, *J. Stat. Phys.* **25**, 619 (1981).
- [38] D. Dhar and S. S. Manna, *Phys. Rev. E* **49**, 2684 (1994).
- [39] D. Dhar, *Phys. Rev. Lett.* **64**, 1613 (1990).
- [40] P. Bak and K. Chen, *Physica D* **38**, 5 (1989).
- [41] F. I. M. Thomas, T. F. Bolton, and A. M. Sastry, *J. Exp. Biol.* **204**, 815 (2001).
- [42] B. E. Layton and A. M. Sastry (unpublished).
- [43] S. Torquato, J. D. Beasley, and Y. C. Chiew, *J. Chem. Phys.* **88**, 6540 (1988).
- [44] Y. C. Chiew and G. Stell, *J. Chem. Phys.* **83**, 761 (1985).
- [45] J. A. Given, I. C. Kim, S. Torquato, and G. Stell, *J. Chem. Phys.* **93**, 5128 (1990).